earth

MDPI

Article

A Scalable GEOBIA Framework for Urban Landscape Monitoring with Sentinel-2 Data: A Case Study in Hue City, Vietnam

Md Abdul Mueed Choudhury [1,*], Giuseppe Modica [2], Salvatore Praticò [3] and Ernesto Marcheggiani [1]

[1] Department of Agricultural, Food and Environmental Sciences, Marche Polytechnic University, 60131 Ancona, Italy; e.marcheggiani@staff.univpm.it
[2] Department of Veterinary Sciences, University of Messina, 98122 Messina, Italy; giuseppe.modica@unime.it
[3] Department of Agriculture, Mediterranea University of Reggio Calabria, 89124 Reggio Calabria, Italy; salvatore.pratico@unirc.it
* Correspondence: m.choudhury@staff.univpm.it

Abstract

The Copernicus Sentinel-2 (S2) data are a crucial resource for urban policymakers in land-cover classification, offering a freely accessible alternative to expensive commercial data sources. While medium spatial resolution often limits the applicability of data-intensive machine learning approaches, the Geographic Object-Based Image Analysis (GEOBIA) framework could be an effective, operational alternative for urban land-cover classification using S2 data. This study applies the Geographic Object-Based Image Analysis (GEOBIA) approach to classify land cover in Hue, Vietnam, using Sentinel-2 data processed through the eCognition interface. The study's findings emphasize the potential of GEOBIA and S2 data in enhancing decision-making processes for city authorities, ensuring better resource allocation, environmental protection, and infrastructure development. The results indicate that the method performs reliably for mesoscale and spatially continuous classes, such as vegetation and built-up surfaces, while accuracy is lower for small or spectrally heterogeneous features, particularly shallow water bodies and fragmented rice paddies, due to mixed-pixel effects inherent in 10–20 m resolution imagery. The results demonstrate an Overall Accuracy (OA) of 91%, highlighting the method's effectiveness in extracting and classifying urban land-cover classes. This study demonstrates a replicable model for urban land monitoring that can be adapted across various geographic contexts. Furthermore, this approach fosters a more data-driven governance model, where urban expansion and land-use changes can be monitored in real time, allowing for proactive interventions. With urbanization accelerating worldwide, particularly in rapidly developing regions, such a cost-effective and accessible classification method can significantly aid in achieving long-term urban sustainability. The findings illustrate the relevance of GEOBIA as a feasible tool for supporting data-driven urban governance, enabling systematic tracking of land-use change, informed infrastructure planning, and sustainable urban management in both developed and rapidly urbanizing regions.

Keywords: urban LULC; GEOBIA; Sentinel-2 data; Hue; Vietnam

Academic Editor: Hariklia D. Skilodimou

Received: 31 January 2026
Revised: 3 March 2026
Accepted: 5 March 2026
Published: 15 March 2026

1. Introduction

An efficient and convenient land cover classification approach is one of the paramount prerequisites to introducing a sustainable monitoring and management system. For city

planners and researchers, convenience is always a massive matter of confrontation when introducing remote-sensing data-based approaches and their applications. Even the most recent features of Remote Sensing (RS), such as hyperspectral imagery and high-spatial-resolution satellite imagery, are being utilized as more effective tools for classification and monitoring the urban land cover, ensuring better accuracy than traditional ones [1–3]. While RS data provides a massive amount of information about terrestrial and land cover data, the tools and techniques are very inconvenient concerning processing skills or expenses [4,5]. Traditional RS-based image classification approaches have predominantly used a pixel-based approach, where the spectral characteristics of each pixel in a satellite image are analyzed separately to classify land cover or objects [6–8]. This approach assumes that each pixel belongs to a homogeneous class, making it suitable for images with coarse spatial resolution. However, this method presents several challenges when applied to high-resolution satellite imagery. Unlike traditional pixel-based classification, GEOBIA does not treat an image as a mere collection of individual pixels. Instead, it first groups pixels into meaningful segments based on similarities in spectral properties, texture, shape, and spatial relationships. Once segmented, these objects are classified using additional criteria such as size, shape, and their relationship to surrounding objects [9–11]. By integrating spatial, spectral, and contextual information, GEOBIA enhances classification accuracy and reduces the salt-and-pepper effect commonly observed in pixel-based approaches. The segmentation process helps preserve object boundaries, making it particularly useful for high-resolution imagery, where land cover features such as buildings, roads, and vegetation patches must be accurately distinguished. Moreover, GEOBIA allows for incorporating advanced classification techniques, including machine learning and rule-based classifiers, further improving accuracy and adaptability. As remote sensing technologies continue to evolve, object-based classification methods like GEOBIA are becoming increasingly important for applications requiring detailed and precise image analysis, such as urban planning, environmental monitoring, and land-use mapping. By overcoming the limitations of pixel-based approaches, GEOBIA represents a more advanced and effective method for high-resolution remote sensing image classification. The GEOBIA approach has also been applied in the case of this study concerning the land cover classification in Vietnam.

Moreover, this case study was introduced as a part of the Italian National Research Project (PRIN) [12] to understand the prospects of designing a geodatabase that combines ground truth and in situ data to bridge the gap between the demand for geospatial information and its availability. The project addresses the increasing demand from the EU and local administrations for in-depth territorial knowledge and aims to serve as a model for data collection in rural areas [13]. This study was also done to understand the utility of the applied approach concerning diversified landscape features in Vietnam, following the previous assessments in different EU cities.

1.1. Objectives

Regarding computing and data acquisition costs, freely accessible multispectral remote sensing data, i.e., Sentinel-2, have been utilized in this study [14–20]. Several studies in Vietnam focused on remote sensing approaches and their applications [21–29]. Most were done to predict or map out the natural disaster-prone areas and vegetation, insisting on landscape change detections and forest monitoring. For instance, recent studies insisted on forest monitoring to understand the landscape changes over time [30–32]. Other studies showed the data fusion approaches to monitor the ecosystem and disaster-prone areas [33–36]. Existing approaches focusing on landscape elements, particularly for urban areas, are hardly available. Also, concerning the Sentinel-2 data, the challenges are yet to be explored, since this data is freely accessible. That is why this case study has been done

in Hue City, assessing the prospects of applying such an approach in Vietnam. Here, the main idea was to introduce an efficient classification approach considering, (i) assessing the potential of free Sentinel-2 data, and (ii) the prospects of the approach in complex urban environments, even for developing countries like Vietnam. The key aspects of this study were to address the following:

The GEOBIA approach could be applicable even with Sentinel-2 data with an acceptable accuracy.

The issues considering the utilization of Sentinel-2 data, i.e., identifying the land-cover class or classes that are mostly affected by spatial limitations.

"Section 2" has been organized to illustrate the methodology in detail, along with the software and data. "Section 3" shows the results discussing the prospects of the applied approach with the relevant references. Overall, this case study could create better scopes for the city authorities to identify and monitor the landscape features, ensuring sustainable land-use management and an urban resilience system.

1.2. Contributions

This study contributes to repositioning and applying GEOBIA with Sentinel-2 as a scalable, policy-ready alternative to data- and expertise-intensive machine learning (ML) frameworks. Most recent urban LULC studies focus on deep learning or ensemble ML models that require large training datasets, extensive parameter tuning, and significant computational infrastructure [37–39]. Previous studies showed that ML models often require massive, high-quality labeled training datasets, which are expensive and time-consuming to produce, and they function as "black boxes," making it difficult for urban planners to adjust the classification logic based on expert knowledge [40–43]. The GEOBIA approach could be more operationally feasible for local authorities as it could be implemented through expert-knowledge rulesets rather than requiring the massive, high-quality training datasets mandated by deep learning [44–46]. For instance, it enables a rule-based approach, which can be directly translated into classification steps (e.g., "if NDVI is low and shape is rectangular, classify as building"). This makes it highly effective for medium-resolution data like Sentinel-2, where it can better mitigate mixed-pixel effects by incorporating neighborhood relationships. This study demonstrates empirically and transparently that a rule-based, object-oriented framework can achieve comparable overall accuracy (91%) using only freely available data and minimal training requirements, even in a complex urban setting. The primary contribution lies in extending the effective use of GEOBIA beyond its conventional reliance on very-high-resolution or commercial imagery, demonstrating that acceptable, operationally robust results can be achieved with medium-resolution (10–20 m) data that are globally accessible. Through a detailed case study of Hue City, Vietnam, where urban-focused remote sensing studies remain limited, the research fills a significant geographic and methodological gap, particularly relevant to developing-country contexts.

2. Materials and Methods

2.1. Dataset

This case study has focused on the urban landscape of Hue City in Vietnam. Hue, formerly known as Thừa Thiên Huế province, is the southernmost coastal city in central Vietnam, roughly at the country's geographic center (Figure 1).

This city is also well-known for the UNESCO-designated temples and imperial palaces, which were also one of the important prospects concerning the landscape classification approach [47–49]. The Sentinel-2 image data (Figure 1) was acquired on January 15, 2023, and downloaded using the Semi-Automatic Classification Plugin (SCP) in QGIS [50]. The Sentinel-2 image data consist of 13 spectral bands with a 10–60 m pixel size (Table 1).

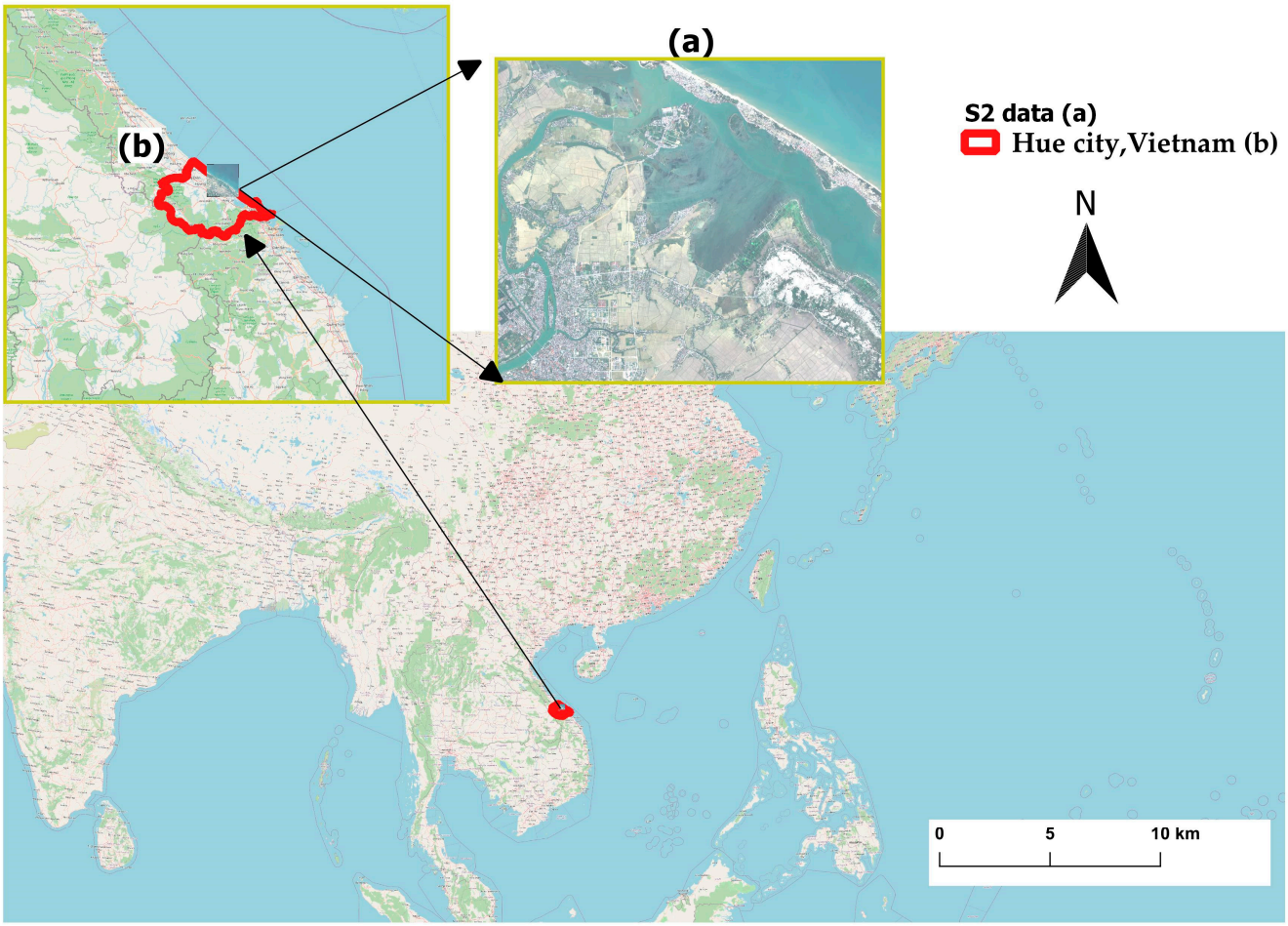

Figure 1. The geographical position of the study area (**a**) and the S2 image data (**b**) in Hue, Vietnam.

Table 1. Thirteen spectral bands from the Sentinel-2 data, ranging from 10 to 60 m pixel size.

Sentinel 2 Bands	Band Parameters		
	Central Wavelength (nm)	Description	Resolution (m)
B1	443	Coastal Blue	60
B2	490	Blue	10
B3	560	Green	10
B4	665	Red	10
B5	705	Visible and Near-Infrared (VNIR)	20
B6-B7-B8-B8a	740–865	VNIR	10–20
B9-B10	940–1375	Short-Wave Infrared (SWIR)	60
B11-B12	1610–2190	SWIR	20

2.2. Methods

The Sentinel-2 (S2) image was exported in Trimble eCognition Developer® 10.2 [51], where the GEOBIA [10,11,52] approach was introduced to extract the information for each landscape feature. The process begins with segmentation, most commonly performed using the Multi-resolution Segmentation (MRS) algorithm, which groups neighboring pixels based on a homogeneity criterion defined by scale, shape, and compactness parameters [53,54]. This creates objects that represent real-world landscape features, effectively mitigating the "salt-and-pepper" noise inherent in pixel-based methods. GEOBIA operates in a multidimensional attribute space. Once objects are formed, the classifier evaluates not only spectral statistics (band means and standard deviations) but also topo-

logical and geometric properties, such as texture, orientation, and hierarchical relationships (e.g., sub-objects vs. super-objects) [55–58]. This enables the use of expert-defined rule sets or k-Nearest Neighbor (KNN) algorithms to distinguish spectrally similar classes. This approach helps preserve the structural integrity of complex urban environments, even with medium-resolution data such as Sentinel-2.

2.2.1. Image Segmentation

Concerning the classification in eCognition, the chessboard segmentation [58] was introduced to initiate the GEOBIA classification approach. The well-known Multiresolution Segmentation (MS) [59] was performed to group contiguous pixels into areas or segments that are homogenous, which is composed of parameters such as the "smoothness/compactness" that determines the preferred shape of parts and the "colour/shape" parameter that controls the weights of spectral and profile information in the calculation of segments' heterogeneity [10,11,59]. Initially, each pixel is treated as an independent object. These pixels are then iteratively merged based on similar measures until more significant homogeneous segments are formed. In eCognition, the Multiresolution Segmentation (MS) algorithm, originally developed by Baatz and Schäpe [60,61], is a bottom-up region-merging approach. It iteratively combines neighboring pixels or objects according to a homogeneity criterion that integrates both spectral (color) and spatial (shape) characteristics. A merger between two objects only occurs if the change in heterogeneity (Δh) is less than the square of the user-defined Scale Parameter (S).

$$\Delta \mathrm{h} < S^2 \tag{1}$$

And the total heterogeneity change (Δh) is a weighted sum of spectral heterogeneity (Δh_{color}) and shape heterogeneity (Δh_{shape}):

$$\Delta h = \omega_{color} \times \Delta h_{color} + (1 - \omega_{color}) \times \Delta h_{shape} \tag{2}$$

where

$$\omega_{color} = \text{ Weight for spectral information}$$

$$(1 - \omega_{color}) = \text{ Weight for shape information } = \text{ "Shape" parameter}$$

Moreover, the 'Compactness' ($\Delta h_{compact}$) parameter is strongly related to the shape heterogeneity (Δh_{shape}) considering the 'Smoothness' (Δh_{smooth}) during the merging of the objects, which can be defined as follows:

$$\Delta h_{shape} = \omega_{compact} \times \Delta h_{compact} + (1 - \omega_{compact}) \times \Delta h_{smooth} \tag{3}$$

where

$$\omega_{compact} = \text{ Weight for compactness information}$$

This method ensures that objects in the image are accurately represented based on spectral and spatial characteristics. One of the main challenges in segmentation is determining optimal parameters, including scale, shape, and compactness. These parameters significantly influence the segmentation outcome. Research has consistently shown that selecting the right values is complex and often relies on a trial-and-error approach [53,54,59,61]. Improper parameter selection can lead to under-segmentation (merging distinct objects) or over-segmentation (dividing a single object into multiple segments) [60,62,63]. Thus, fine-tuning these settings is crucial to achieving accurate and meaningful segmentation for further image analysis.

For this study, five scale parameters, i.e., 20, 40, 60, 80 and 100 [46,63–65] have been tested with the shape and compactness weight [Table 2]. Table 2 shows the mathematical relationship between the Scale Parameter (SP) and the structural integrity of image objects derived from Sentinel-2 data. Selecting Scale 20 as the optimal parameter is justified because it yields the lowest Intra-object Spectral Variance, keeping segments spectrally "pure" and preventing them from bleeding into neighboring land-cover classes. At this scale, the Mean Object Size aligns closely with the minimum mapping unit required for fragmented landscapes, such as narrow irrigation canals or small heritage sites, which would otherwise be lost to under-segmentation at higher scales (e.g., SP 60 or 100).

Table 2. Testing the segmentation with parameters.

Scale Parameter	No. of Objects	Mean Object Size (Pixels)	Over-Seg Ratio (OSn)	Under-Seg Score (Visual)	Intra-Object Variance (NIR Band)
20	~18,500	~12.5	4.8	1 (None)	3.12
40	~8200	~35.2	2.4	2 (Low)	7.45
60	~3400	~78.6	1.1	3 (Moderate)	14.80
80	~1200	~145.3	0.4	4 (High)	28.30
100	~650	~260.8	0.2	5 (Extreme)	42.15

The Over-segmentation Ratio (OSn)is calculated by dividing the total number of objects generated at a specific scale by the number of manually delineated reference polygons. A ratio significantly higher than 1.0 (as seen at Scale 20) indicates that a single real-world feature has been split into many smaller segments, while a ratio moving toward 0.1 suggests the opposite effect, where multiple distinct features are merged into one. This metric is vital for determining the "optimal" scale where objects are neither too fragmented nor too generalized for the 10m Sentinel-2 resolution.

For the shape and compactness weight, the values starting from 0.1 to 0.9 have been tested simultaneously with each of the five scale parameters (i.e., Table 2). After several attempts, the ideal values utilized for segmentation were found as scale parameter = 20, shape = 0.5, and compactness = 0.5 [Figure 2]. Setting both Shape and Compactness to 0.5 reflects a balanced priority between spectral information and geometric regularity. A Shape value of 0.5 prevents the segmentation from being overly influenced by spectral noise or "salt-and-pepper" effects common in 10m pixels, providing segments with defined boundaries essential for identifying linear features like streets. Simultaneously, a Compactness value of 0.5 acts as a moderating force; it allows the algorithm to capture elongated, natural shapes like riverbanks while preventing them from becoming too fractal or "branchy," which can occur when compactness is set too low. This configuration, Scale 20 with balanced shape/compactness, minimizes the Under-segmentation Visual Score, preserving high-contrast boundaries (such as the interface between "Wet & Turbid Soil" and "Vegetation").

Concerning the resolution, the MS algorithm has been used to segment the image data with homogeneous objects. The resulting MS shows that several polygons have been created where the classification approach could be applied to extract the specific land use classes [Figure 2]. Regarding land cover classification, each polygon or object possesses several characteristics that aid its classification, including spectral, geometric, spatial, topological, and hierarchical attributes [a complete table with the segmentation parameters have been added to the Supplementary Materials].

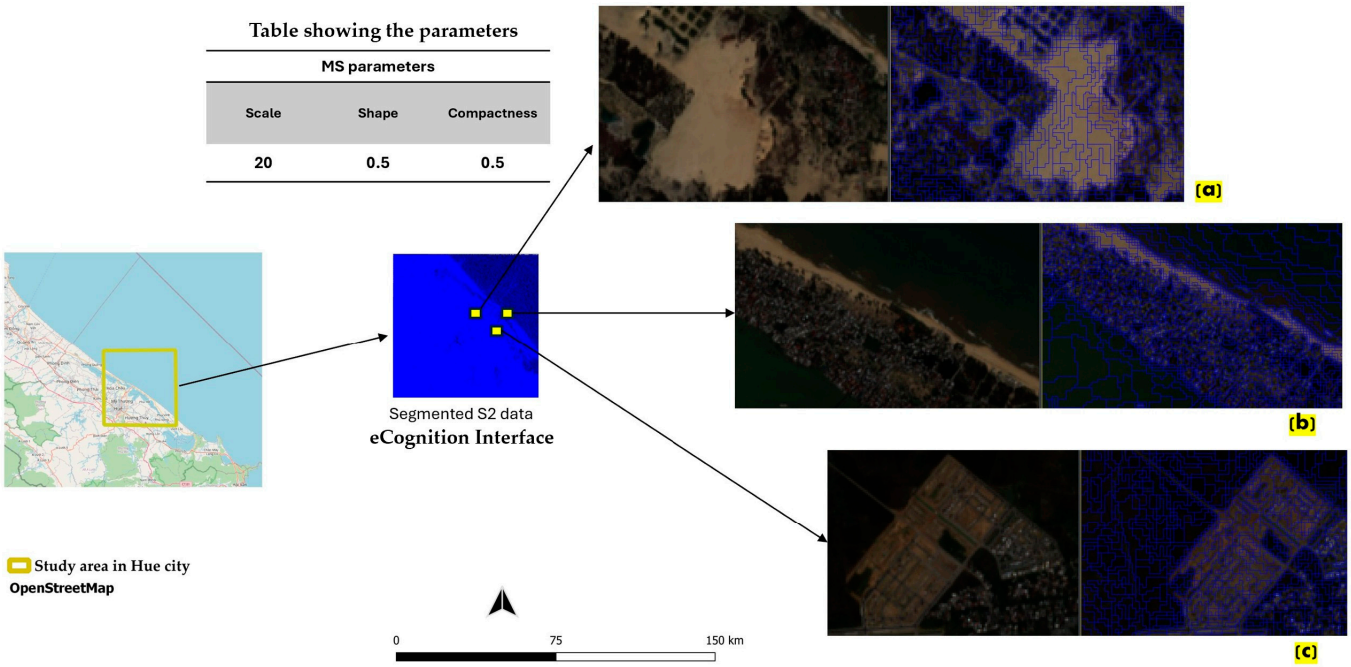

Figure 2. MS and parameters of S2 data on eCognition (interface). (**a**–**c**) show the segmented polygons (**right**) for the image data (**left**).

2.2.2. Image Classification

Spectral attributes relate to color and intensity, while geometric properties define an object's shape, size, and compactness. Spatial attributes describe the object's position and relationship with surrounding elements, whereas topological features consider connectivity and adjacency within the image. Hierarchical attributes establish relationships between objects at different levels, such as a building within a city. These characteristics, known as features, are measurable properties like color, texture, or shape, which play a crucial role in object classification [65–68]. By analyzing the feature values, a classification system can categorize an object into a specific class, such as differentiating water bodies from vegetation or buildings from roads in satellite imagery. The effectiveness of classification depends on selecting relevant features, as distinct feature combinations enable accurate identification of objects. Here, three parameters were calibrated, which can be defined as follows,

Normalized Difference Vegetation Index,

$$\mathrm{NDVI} = (\mathrm{NIR} - \mathrm{RED})/(\mathrm{NIR} + \mathrm{RED}) \quad (4)$$

Normalized Difference Water Index,

$$\mathrm{NDWI} = (\mathrm{NIR} - \mathrm{SWIR})/(\mathrm{NIR} + \mathrm{SWIR}) \quad (5)$$

Bare Soil Index,

$$\mathrm{BSI} = ((\mathrm{Red} + \mathrm{SWIR}) - (\mathrm{NIR} + \mathrm{Blue}))/((\mathrm{Red} + \mathrm{SWIR}) + (\mathrm{NIR} + \mathrm{Blue})) \quad (6)$$

where NIR = Near-Infrared, SWIR = Short-Wave Infrared.

These parameters have been calibrated for each object in the segmented image to develop the rule set for extracting spectral information for each class (Figure 3).

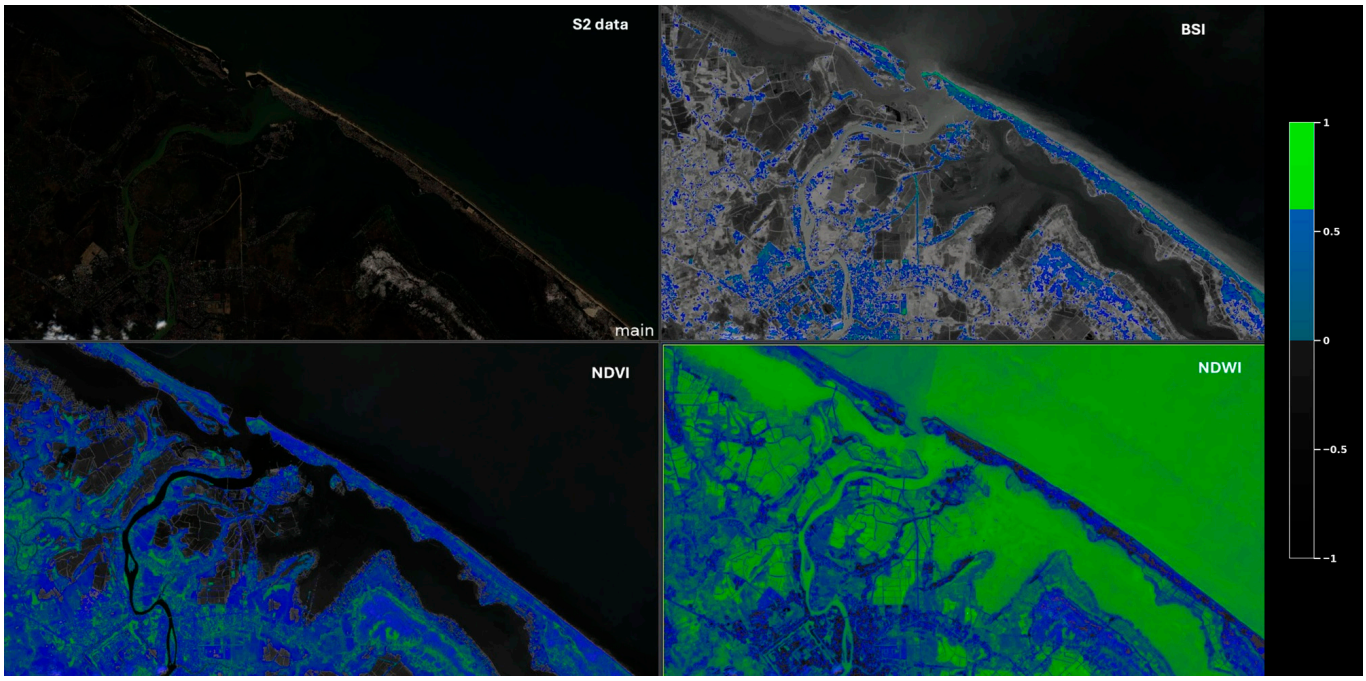

Figure 3. The calibrated index features and the S2 data (**upper left**) on eCognition.

The NDVI, NDWI, and BSI were considered because they could represent the three fundamental "endmembers" of the urban environment: green biomass, water, and impervious/bare surfaces. In a Geographic Object-Based framework, these indices provide the primary spectral evidence needed to separate complex classes that often overlap in raw bands. Specifically, NDVI is essential for isolating the "Vegetation" class by exploiting the high contrast between the red absorption and near-infrared (NIR) reflection of chlorophyll. NDWI is critical for delineating "Water Resources" as it enhances the water's signal while suppressing soil and vegetation noise, which is particularly vital for detecting turbid river systems in tropical cities like Hue. Finally, BSI is superior to simple urban indices because it can distinguish between "Urban Built" surfaces and "Wet & Turbid Soil" by combining the Blue, Red, NIR, and Short-Wave Infrared (SWIR) bands. While other indices like the Normalized Difference Built-up Index (NDBI) exist, they often confuse bright fallow land with concrete; the combination of NDVI, NDWI, and BSI provides a comprehensive "V-I-S" (Vegetation–Impervious–Soil) framework. The BSI enhances surfaces characterized by exposed soil and impervious materials; higher BSI values highlight these surfaces, while lower values correspond to vegetation and water. The NDVI emphasizes vegetated areas, with high values indicating healthy vegetation such as parks, agricultural fields, and urban green spaces, and low or negative values identifying impervious surfaces and water. And so on, the higher NDWI values clearly highlight rivers, coastal waters, and wetlands, while lower values correspond to built-up and vegetated areas. In this case of the GEOBIA approach, these feature values have been utilized to generate spatially meaningful objects or polygons. These object-level statistics derived from the indices enable robust discrimination between the land cover patches, especially in the case of heterogeneous urban landscapes [67,69]. For instance, NDVI-customized feature values have been utilized to differentiate the vegetated and non-vegetated areas. For each polygon, the values have been tested using the "Update range" option on the object feature algorithm on eCognition. To develop the ruleset, the value range was NDVI $\leq$ 0.24 and NDVI $\geq$ 0.25 for the non-vegetated and vegetated classes, and so on, and have been tested and specified for other index features. While the landcover classes could be assigned utilizing the index-features, there were issues with other segmented objects, like clouds and their shadows, interfering

with the classes. To refine the errors, it was necessary to exclude the clouds even before running the classification algorithm. And for this, the other spectral features and respective statistical analysis, i.e., 'Brightness', 'Maximum difference', and 'Standard Deviation' have been tested and checked for the objects. Once the value-range has been well specified for each object, the next step is to prepare the ruleset, performing the most suitable choice of the algorithm in eCognition [51,70,71]. Regarding the ranges of the feature values, the "Assign class" algorithm was applied to classify each object. This algorithm operates on Boolean logic or Fuzzy logic thresholds, where it evaluates the condition $\mathbb{C}$ for the image object o. If the condition is met, the object is assigned to the class $\mathcal{L}$.

$$f(o) = \begin{cases} \mathcal{L} & if\ X(o) \in [T_{min},\ T_{max}] \\ unclassified & otherwise \end{cases} \quad (7)$$

where

$X(o)$ = value of a specific feature (e.g., NDVI, NDWI, Brightness, etc.) for object o;

$[T_{min},\ T_{max}]$ = threshold range defined in the "Condition" parameter.

This algorithm evaluates each image object sequentially and checks whether it satisfies the rule set associated with a target class; if the conditions are fulfilled, the object is assigned to that class [Ruleset has been added to the Supplementary Materials]. It can assign classes based on spatial relationships, such as proximity to other classes, containment, or relative border lengths, making it particularly powerful for context-aware classification [14,71,72]. In this case, this algorithm was also applied to extract information for each object by considering the range of the values for each feature relative to the spectral response of the object. And thus, the resulting land cover classes have been identified. Later, the classification results were validated and exported to QGIS as a unique shapefile for further visualization and mapping interpretations.

2.2.3. Validation

The Google Earth Pro (GEP) image data [66,71,73,74] were used to validate the classification results, as no field data were available for the target area. GEP image data with a high resolution and the real-time 3D visual facility have become one of the most reliable data sources, especially for validating the land cover classification outcomes [75–78]. The data quality has made it possible for the human eye to detect the objects concerning the diversified land cover classes. The validation process was performed in the eCognition platform, utilizing confusion matrices to compare true classes with those assigned by the classifier on the generated maps [13,14,59]. Initially, 100 to 150 samples/class have been randomly chosen from the GE covering the whole study area in Hue, Vietnam as the "true samples". A stratified random sampling approach was applied to ensure proportional representation of each land-cover class across the entire study area (Figure 4). Between 100 and 150 validation samples (N number of reference points/class in Table 3) per class were generated using QGIS, where a minimum separation distance of 30 m to 60 m (considering the Sentinel-2 pixels) was enforced between validation points, reducing the spatial autocorrelation. Once these samples were exported to eCognition, they were integrated into an Object-Based Image Analysis (OBIA) framework.

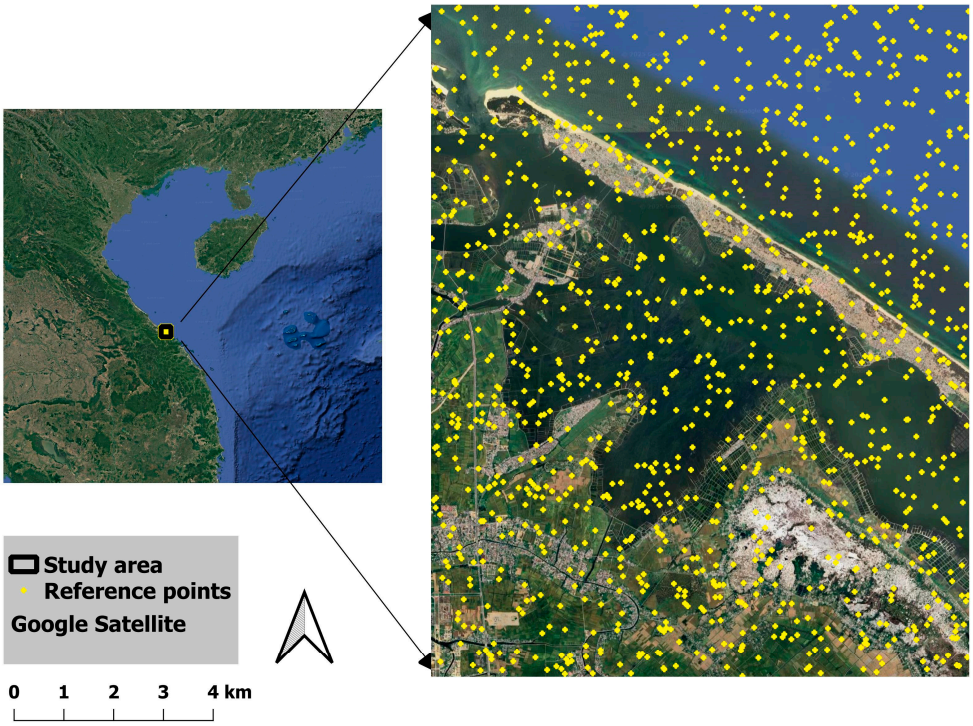

Figure 4. Reference points in the study area for validation.

Table 3. Validation results for the identified land cover classes.

	Vegetation (N* = 135)	Water Resources (N* = 110)	Urban Built (N* = 150)	Wet and Turbid Soil/Rice Cultivated Area (N* = 100)
PA [1]	0.97	0.24	0.97	0.11
UA [1]	0.98	0.11	0.85	0.48
Hellden	0.98	0.15	0.91	0.18
KIA per Class	0.93	0.23	0.96	0.11

[1] PA = Producer's Accuracy, UA = User's Accuracy, N* = number of reference points.

Unlike traditional pixel-based methods, eCognition requires converting point or polygon samples into discrete image objects created during the segmentation phase. This step is vital because the software uses the k-Nearest Neighbor (KNN) algorithm to categorize the landscape based on these training inputs. The final confusion matrix is generated by a rigorous comparison between the "Actual objects" (the validated true samples) and the "Predicted samples" (the results of the KNN classification). This methodology ensures that the accuracy assessment reflects the algorithm's true performance across diverse classes, such as vegetation and urban built-up areas, while accounting for the unique spectral and geometric properties of segmented objects rather than isolated, independent pixels. By using the KNN-based matrix, the study provides a reliable measure of how well the spectral signatures of Sentinel-2 data were translated into a representative land-cover map of the region.

The confusion matrix [Table 3] provides a comprehensive evaluation of classification performance by integrating class-wise and overall accuracy metrics. Producer's Accuracy (PA) measures the completeness of the classification by quantifying omission error, indicating how effectively reference samples of a given class are correctly identified in the map. In this study, PA is very high for Vegetation (0.97) and Urban built (0.97), demonstrating strong detection capability for these dominant classes. In contrast, Water resources (0.24) and

Wet and turbid soil/rice cultivated areas (0.11) show very low PA, indicating substantial omission errors likely caused by mixed pixels and spectral overlap in transitional environments. User's Accuracy (UA), which reflects commission error and therefore the reliability of mapped classes, follows a similar pattern: Vegetation shows excellent reliability (0.98), and Urban built remains robust (0.85), whereas Water resources (0.11) and Wet/turbid soil (0.48) display weaker reliability, suggesting notable class confusion.

The PA derived from the confusion matrix [Table 3] quantifies the completeness of the results by measuring the proportion of actual ground features correctly identified by the classifier, thereby accounting for omission errors. The UA serves as a metric of correctness, indicating the map's reliability by determining how often a pixel assigned to a specific class actually represents that category on the ground, thereby highlighting commission errors. The Hellden parameter is also used to determine the mean accuracy of each class. The mean accuracy for each class 'i' can be calculated using the equation as follows [79]:

$$\text{Mean accuracy (i)} = \frac{2A}{B+C}100\%$$

where A is the number of correctly classified reference points for class i, B is the total number of reference points in class i in the reference data, and C is the total number of reference points classified into class i.

The Kappa Index of Agreement (KIA), or Cohen's kappa coefficient, is a robust statistical metric used to evaluate classification performance by measuring the proportion of agreement that occurs beyond mere random chance. Unlike simple percentage calculations, the Kappa value provides a more nuanced assessment: a value of 1 signifies perfect alignment between the classifier and ground truth, whereas lower values indicate diminishing levels of agreement. In cases of significant systematic error, the coefficient can even become negative, reflecting disagreement greater than what would be expected by chance. Complementing this, Overall Accuracy (OA) offers a broad perspective on the entire dataset by calculating the ratio of correctly classified diagonal cells in the confusion matrix to the total number of samples. Together, these metrics ensure that the final land-cover map is both statistically significant and reliable across all identified biocultural landscape categories.

3. Results

The GEOBIA approach applied in this study has been used as an efficient technique, even in the case of Sentinel-2 data, which has a cloud coverage of almost 30% with a coarse resolution. The main land cover classes were identified as follows:

- Wet and turbid soil/rice cultivated area;
- Urban built;
- Vegetation;
- Water resources.

The classification of the land cover (Figure 5) features, such as Vegetation and Water resources, were more significant than the other classes. For instance, the urban gray infrastructures were classified as unique objects as "Urban built" where it was not possible to extract diversified land cover classes. This was mostly because of mixed segmentation during the classification due to the quality of the Sentinel-2 data [14,80,81].

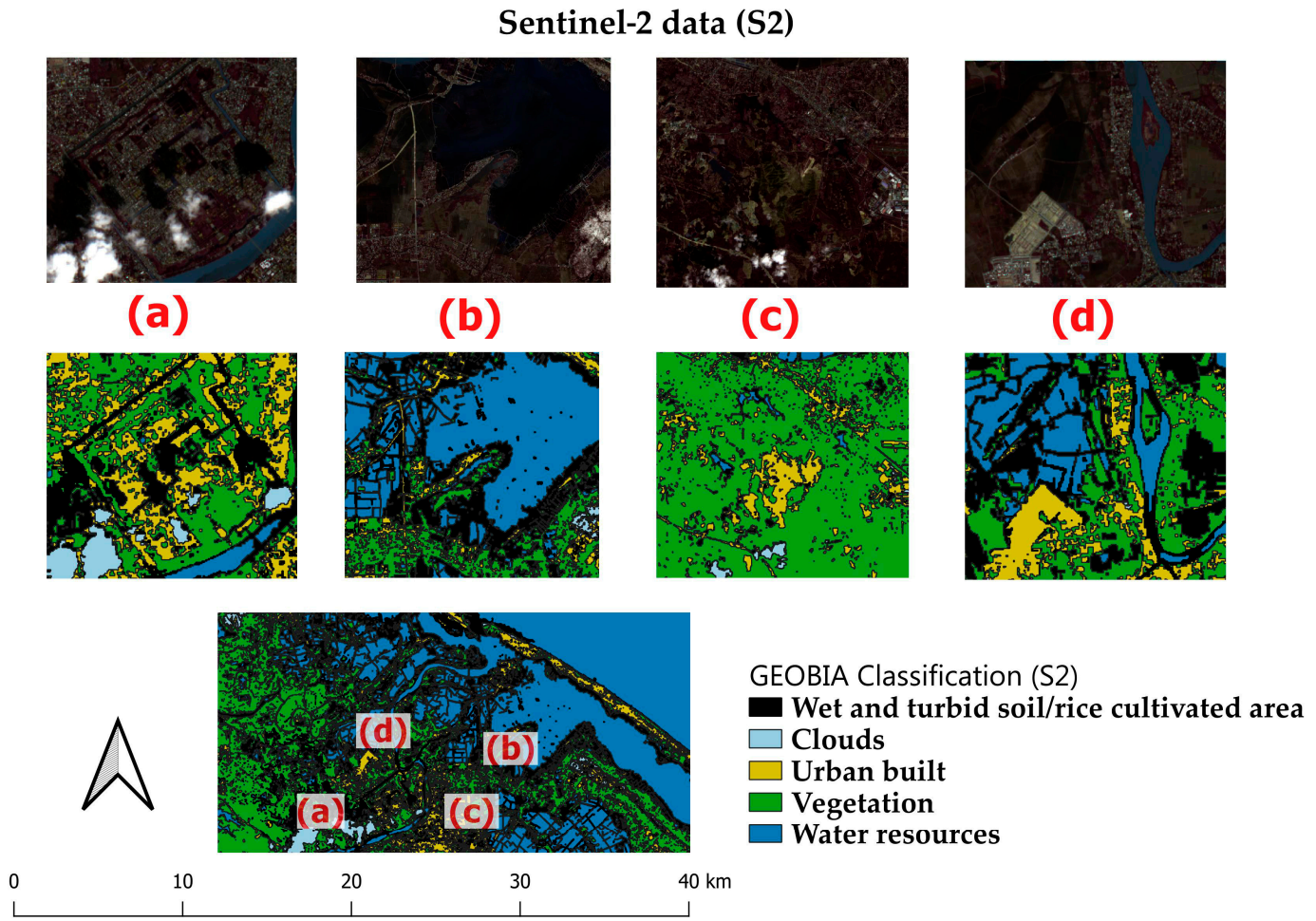

Figure 5. Urban landscape classification utilizing Sentinel-2 data in eCognition. The (**a**–**d**) are representing the different places to show the results (Zoomed).

The validation results in Table 3 show an overall accuracy of 91%, where the KIA percentage was 83%. The Confusion matrix includes specialized indices like the Hellden Index, a mean accuracy measure denoting the probability of a random point matching between the estimated and ground-truth classes. While Overall Accuracy (OA) provides a global percentage of correctly classified samples, Kappa Statistic (or Kappa per class) is frequently used to measure the agreement beyond what would be expected by chance. The Vegetation and Urban built classes showed higher Producer's Accuracy (PA) of 97% and 98%, respectively [Figure 6]. This indicates that the segmentation and classification rules successfully captured nearly all instances of these features in the imagery. However, the Water resources and Wet and turbid soil classes demonstrated lower performance in either case of PA and UA. These issues could be attributed to several spatial and spectral limitations inherent to Sentinel-2 data, especially when dealing with mixed environments.

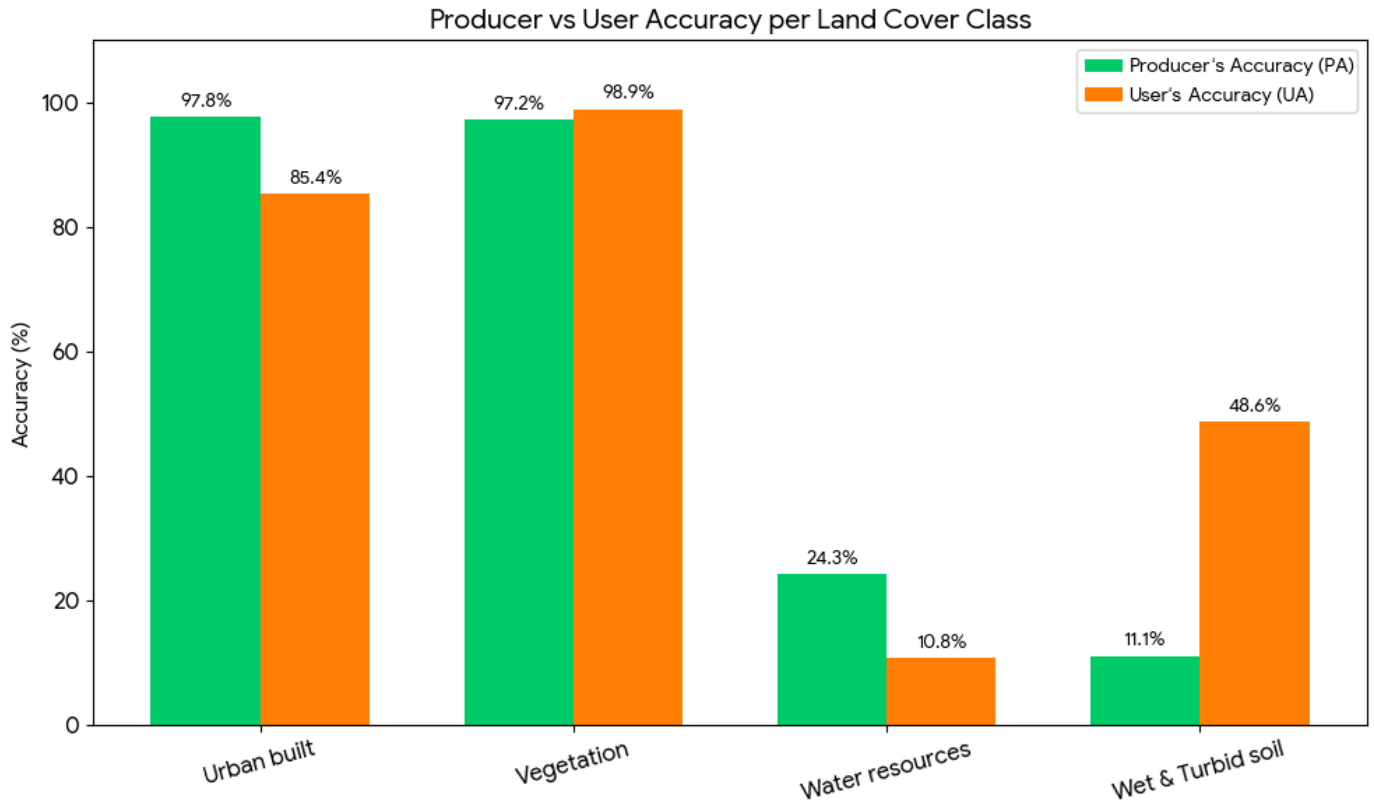

Figure 6. The Producer's Accuracy (PA) and User's Accuracy (UA) for each class.

The coarse resolution of Sentinel-2 (10 m, 20 m, or 60 m, depending on the band) creates a "Mixed Pixel" issue. In transition zones, a single pixel may contain both shallow water and shoreline vegetation. Because the pixel records an average reflectance, the classifier often struggles to assign it to a single class, leading to the omission errors found in Producer's Accuracy (PA) for Water resources (24.29%) and Wet and turbid soil (11.11%) [Table 4].

Table 4. Comparison of the performance matrix during the validation.

Feature Detail	Impact on Accuracy	Confusion Matrix Results
Small Water Bodies	Pixel size exceeds feature size	Low PA (24.29%)
Soil Moisture	Spectral overlaps with urban shadows	Low UA (48.64%)
Turbidity	Increased reflectance mimics land	High Confusion

4. Discussion

In this study, S2 data proves reliable for meso-scale urban structure mapping but faces significant technical limitations when applied to micro-scale features. Specifically, the framework is unsuitable for identifying small water bodies under 0.05 hectares or narrow irrigation canals because the 10 m to 20 m spatial resolution leads to severe mixed-pixel effects, where the spectral signature of water is contaminated by surrounding land cover. That is why the S2 data are primarily recommended for vegetation mapping and built-up detection [37,38,82], where features are spatially continuous and distinct. For aquatic features, it is effective only for large water bodies exceeding 3–4 contiguous 10m pixels, ensuring the objects formed during segmentation are spectrally pure. This distinction is crucial for researchers to avoid under-segmentation errors and ensure that the chosen

scale parameter aligns with the physical dimensions of the target landscape elements. The classification outcomes recognize the issues of utilizing Sentinel-2 data, while illustrating the possibility of land cover monitoring concerning the basic landscape features. Previous studies suggest the integration of the Sentinel-2 data, especially for the accurate delineation of landscape features confronting issues like the 'Urban Built' class [83–85].

Moreover, S2 image data struggle to resolve fine-grained urban morphology because the 10–20 m pixel size is inherently too coarse to capture narrow streets, small courtyards, and fine-gridded building patterns [86,87]. These features become spatially smoothed or disappear altogether when aggregated to coarser resolutions, exacerbating the loss of urban detail noted in several urban remote sensing studies [88–92]. Recent work on urban change and built-up extraction also tends to integrate Sentinel-2 with Sentinel-1 or commercial VHR sensors, or to use deep learning frameworks that explicitly account for mixed-pixel behavior, yet these approaches still acknowledge that the fundamental spatial resolution limit of Sentinel-2 prevents accurate representation of very detailed urban features and narrow street canyons, restricting its role to meso-scale urban structure and spatio-temporal trend analysis rather than precise intra-urban mapping [93–98]. The potential barriers to adopting those techniques include, but are not limited to, the level of specialist knowledge, the data collection time, instrument types and parameters for the acquisitions, and so on, especially for public authorities. For instance, there are studies available [99–103] with better accuracy utilizing LiDAR and multispectral commercial satellite data, which are hardly cost-efficient and also require higher processing tools and skills. Studies are evident that the high-resolution commercial data (i.e., Rapid Eye, IKONOS, Geo-eye) are available with an approximate cost of 1–14 € per km^2, while LiDAR data (62–240 € per km^2) are the most expensive for such kind of studies [95,96]. This study utilizes Sentinel-2 data, which is freely available and could be utilized anywhere, especially for public authorities. Concerning the cost-efficiency and the prospective applications, this study has been conducted to illustrate the possibilities of replicating the approach. This classification approach could provide strong evidence, which could also be tested with the commercially available data with better resolution [97–100].

This study aims to highlight the cost-efficiency and replicability of the proposed classification approach, demonstrating its potential as a sustainable and scalable solution for landscape monitoring and urban planning. By leveraging freely available data, the approach minimizes the expenses associated with traditional data collection and monitoring systems, making it a viable alternative for resource-limited municipalities. Since the approach relies on freely accessible data, it offsets costs associated with data acquisition while maintaining a stable and efficient monitoring system, ultimately leading to increased management efficiency. The application of the GEOBIA approach will provide planners with a systematic method for evaluating and monitoring the urban landscape for the long-term sustainability of various developmental projects [101–103]. By adopting this approach, policymakers can implement strategies that align with sustainable development goals, ensuring a balance between economic growth and environmental as well as historic landscape conservation [104,105]. In summary, the study shows the significance of a cost-effective, data-driven classification system that could enhance urban planning efficiency, improve landscape monitoring, and strengthen decision-making processes. The integration of free and high-resolution commercial data ensures that the approach remains adaptable and scalable, providing city authorities with a powerful tool for sustainable policymaking.

5. Conclusions

This study presents a practical and accessible framework for land-cover mapping in complex urban environments, with particular emphasis on affordability, transparency, and operational feasibility. Rather than relying on expensive commercial imagery, LiDAR datasets, or computationally intensive machine learning architectures, the proposed approach demonstrates how freely available Sentinel-2 data combined with a rule-based Geographic Object-Based Image Analysis (GEOBIA) workflow can provide meaningful classification outputs in heterogeneous tropical cities. The findings suggest that the approach performs consistently for spatially continuous and meso-scale classes such as vegetation and built-up areas. These categories benefit from clearer spectral separability and larger object extents relative to the 10–20 m pixel size. In contrast, smaller or spectrally mixed features such as narrow canals, shallow water bodies, and fragmented rice-cultivated or wet soil areas remain challenging to delineate accurately. These limitations are primarily attributable to mixed-pixel effects and spectral overlap in transitional urban–peri-urban environments. The method offers advantages in terms of cost efficiency, transparency of rule-based classification, and reproducibility, which may be particularly relevant for local administrations operating under financial and technical constraints. The workflow is reproducible, computationally manageable, and adaptable to other cities with similar morphological complexity, making it suitable for broader implementation in data-limited contexts. Furthermore, while the current study focuses on a single-date feasibility assessment, the framework is inherently extensible. Future developments may incorporate multi-temporal composites to better capture seasonal variability, integrate Synthetic Aperture Radar (SAR) data to improve discrimination of moisture-related classes, or combine rule-based segmentation with supervised machine-learning classifiers to enhance separability in spectrally ambiguous areas. Algorithm refinement, threshold optimization, and cross-city validation would further strengthen scalability and robustness. Overall, the study positions medium-resolution GEOBIA not as a replacement for high-resolution or advanced analytical systems, but as a pragmatic, transparent, and economically sustainable alternative capable of supporting continuous urban land-cover monitoring and contributing to more informed and sustainable land-use governance.

Supplementary Materials: The following supporting information can be downloaded at: https://www.mdpi.com/article/10.3390/earth7020051/s1, A complete ruleset/script (dpr file) and the segmentation trial table have been attached as Supplementary Materials.

Author Contributions: Conceptualization, M.A.M.C. and E.M.; methodology, software, validation, formal analysis, investigation, M.A.M.C.; resources, data curation, S.P., G.M. and E.M.; writing—original draft preparation, M.A.M.C. and E.M.; writing—review and editing, M.A.M.C., G.M., S.P. and E.M.; visualization, M.A.M.C., G.M. and S.P.; supervision, G.M., S.P. and E.M. All authors have read and agreed to the published version of the manuscript.

Funding: This research was funded by the Ministry of University and Research (MUR) Italy, project PRIN Eye-Land: A crowd-sensing geospatial database for the monitoring of rural areas-Prot. 2020EMLWTN 2020EMLWTN_006 CUP: I53C22000430001, by the MUR D.D. notice no. 1628 of 10/16/2020—PRIN 2020.

Data Availability Statement: The original contributions presented in the study are included in the article/Supplementary Materials, further inquiries can be directed to the corresponding author.

Acknowledgments: We thank the anonymous reviewers for their constructive, detailed, and helpful comments.

Conflicts of Interest: The authors declare no conflicts of interest.

Abbreviations

The following abbreviations are used in this manuscript:

BSI	Bare Soil Index
GEE	Google Earth Engine
GEOBIA	Geographic Object-Based Image Analysis
GIS	Geographic Information System
GSD	Ground sampling distance
KIA	Kappa Index of Agreement
KNN	k-Nearest Neighbor
LULC	Land Use and Land Cover
ML	Machine learning
NDVI	Normalized Difference Vegetation Index
NDWI	Normalized Difference Water Index
OA	Overall Accuracy
PA	Producer's Accuracy
PRIN	Progetti di Rilevante Interesse Nazionale (Projects of Relevant National Interest, Italy)
SAR	Synthetic Aperture Radar
UA	User's Accuracy
VHR	Very-high resolution

References

1. de Pinho, C.M.D.; Fonseca, L.M.G.; Korting, T.S.; de Almeida, C.M.; Kux, H.J.H. Land-cover classification of an intra-urban environment using high-resolution images and object-based image analysis. *Int. J. Remote Sens.* **2012**, *33*, 5973–5995. [CrossRef]
2. Ai, J.; Zhang, C.; Chen, L.; Li, D. Mapping annual land use and land cover changes in the Yangtze Estuary Region using an object-based classification framework and landsat time series data. *Sustainability* **2020**, *12*, 659. [CrossRef]
3. He, S.; Du, H.; Zhou, G.; Li, X.; Mao, F.; Zhu, D.; Xu, Y.; Zhang, M.; Huang, Z.; Liu, H.; et al. Intelligent Mapping of Urban Forests from High-Resolution Remotely Sensed Imagery Using Object-Based U-Net-DenseNet-Coupled Network. *Remote Sens.* **2020**, *12*, 3928. [CrossRef]
4. How Much Does LIDAR Mapping Cost?—Queensland Drones. Available online: https://qlddrones.com.au/blog/how-much-does-lidar-mapping-cost/ (accessed on 28 November 2022).
5. Shao, T.; Qu, Y.; Du, J. A low-cost integrated sensor for measuring tree diameter at breast height (DBH). *Comput. Electron. Agric.* **2022**, *199*, 107140. [CrossRef]
6. Fuller, R.M.; Groom, G.B.; Jones, A.R. The land-cover map of great Britain: An automated classification of landsat thematic mapper data. *Photogramm. Eng. Remote Sens.* **1994**, *60*, 553–562.
7. Turner, M.D.; Congalton, R.G. Classification of multi-temporal SPOT-XS satellite data for mapping rice fields on a West African floodplain. *Int. J. Remote Sens.* **1998**, *19*, 21–41. [CrossRef]
8. Gao, J.; Skillcorn, D. Capability of SPOT XS data in producing detailed land cover maps at the urban-rural periphery. *Int. J. Remote Sens.* **1998**, *19*, 2877–2891. [CrossRef]
9. Vannier, C.; Hubert-Moy, L. Detection of wooded hedgerows in high resolution satellite images using an object-oriented method. In *IGARSS 2008–2008 IEEE International Geoscience and Remote Sensing Symposium*; IEEE: Boston, MA, USA, 2008.
10. Choudhury, M.A.M.; Marcheggiani, E.; Galli, A.; Modica, G.; Somers, B. Mapping the Urban Atmospheric Carbon Stock by LiDAR and WorldView-3 Data. *Forests* **2021**, *12*, 692. [CrossRef]
11. Choudhury, M.A.M.; Marcheggiani, E.; Despini, F.; Costanzini, S.; Rossi, P.; Galli, A.; Teggi, S. Urban Tree Species Identification and Carbon Stock Mapping for Urban Green Planning and Management. *Forests* **2020**, *11*, 1226. [CrossRef]
12. EYE-LAND PROJECT—EyeLand. Available online: https://prineyeland.it/about-us/ (accessed on 26 July 2025).
13. Eye-Land App—Database Geospaziale Basato Sul Crowd-Sensing. Available online: https://eyeland-app.uniud.it/ (accessed on 26 July 2025).
14. Petrushevsky, N.; Manzoni, M.; Monti-Guarnieri, A. Fast Urban Land Cover Mapping Exploiting Sentinel-1 and Sentinel-2 Data. *Remote Sens.* **2021**, *14*, 36. [CrossRef]
15. Shafizadeh-Moghadam, H.; Minaei, F.; Talebi-khiyavi, H.; Xu, T.; Homaee, M. Synergetic use of multi-temporal Sentinel-1, Sentinel-2, NDVI, and topographic factors for estimating soil organic carbon. *Catena* **2022**, *212*, 106077. [CrossRef]

16. Zhou, T.; Geng, Y.; Chen, J.; Pan, J.; Haase, D.; Lausch, A. High-resolution digital mapping of soil organic carbon and soil total nitrogen using DEM derivatives, Sentinel-1 and Sentinel-2 data based on machine learning algorithms. *Sci. Total Environ.* **2020**, *729*, 138244.
17. Cai, Y.; Lin, H.; Zhang, M. Mapping paddy rice by the object-based random forest method using time series Sentinel-1/Sentinel-2 data. *Adv. Space Res.* **2019**, *64*, 2233–2244.
18. Jacob, A.W.; Vicente-Guijalba, F.; Lopez-Martinez, C.; Lopez-Sanchez, J.M.; Litzinger, M.; Kristen, H. Sentinel-1 InSAR Coherence for Land Cover Mapping: A Comparison of Multiple Feature-Based Classifiers. *IEEE J. Sel. Top. Appl. Earth Obs. Remote Sens.* **2020**, *13*, 535–552. [CrossRef]
19. Sica, F.; Pulella, A.; Nannini, M.; Pinheiro, M.; Rizzoli, P. Repeat-pass SAR interferometry for land cover classification: A methodology using Sentinel-1 Short-Time-Series. *Remote Sens. Environ.* **2019**, *232*, 111277. [CrossRef]
20. Praticò, S.; Solano, F.; Di Fazio, S.; Modica, G. Machine learning classification of mediterranean forest habitats in google earth engine based on seasonal sentinel-2 time-series and input image composition optimisation. *Remote Sens.* **2021**, *13*, 586. [CrossRef]
21. Ni, T.N.K.; Tin, H.C.; Thach, V.T.; Jamet, C.; Saizen, I. Mapping Submerged Aquatic Vegetation along the Central Vietnamese Coast Using Multi-Source Remote Sensing. *ISPRS Int. J. Geo-Inf.* **2020**, *9*, 395. [CrossRef]
22. Hoang, T.T.; Truong, V.T.; Hayashi, M.; Tadono, T.; Nasahara, K.N. New JAXA High-Resolution Land Use/Land Cover Map for Vietnam Aiming for Natural Forest and Plantation Forest Monitoring. *Remote Sens.* **2020**, *12*, 2707. [CrossRef]
23. Pham, N.T.T.; Nguyen, C.T.; Vu, H.H. Assessing and modelling vulnerability to dengue in the Mekong Delta of Vietnam by geospatial and time-series approaches. *Environ. Res.* **2020**, *186*, 109545. [CrossRef]
24. Nguyen, H.H.; Nguyen, H.T.T.; Tran, L.T.N.; Bohm, S.; Nghia, N.H.; Le, A.T.; Duong, L.V.K.; Furniss, M.J. Classification Methods for Mapping Mangrove Extents and Drivers of Change in Thanh Hoa Province, Vietnam during 2005–2018. *For. Soc.* **2020**, *4*, 225–242. [CrossRef]
25. Xia, J.; Yokoya, N.; Pham, T.D. Probabilistic Mangrove Species Mapping with Multiple-Source Remote-Sensing Datasets Using Label Distribution Learning in Xuan Thuy National Park, Vietnam. *Remote Sens.* **2020**, *12*, 3834. [CrossRef]
26. Minh, V.Q.; Quang, T.C.; Du, T.T.; Hien, T.T. Spatial Delineation of Rice Yield and Production by the Combination of Rice Crop Modelling and Remote Sensing: A Case Study in Soc Trang Province, Vietnam. *Int. J. Adv. Sci. Eng. Inf. Technol.* **2021**, *11*, 856–863. [CrossRef]
27. Nguyen, H.H.; Vu, H.D.; Röder, A. Estimation of Above-Ground Mangrove Biomass Using Landsat-8 Data- Derived Vegetation Indices: A Case Study in Quang Ninh Province, Vietnam. *For. Soc.* **2021**, *5*, 506–525. [CrossRef]
28. Nguyen, T.T.Q.; Takeuchi, W.; Misra, P.; Sachiko, H. Technical note: Emission mapping of key sectors in Ho Chi Minh City, Vietnam, using satellite-derived urban land use data. *Atmos. Chem. Phys.* **2021**, *21*, 2795–2818. [CrossRef]
29. Maskell, G.; Chemura, A.; Nguyen, H.; Gornott, C.; Mondal, P. Integration of Sentinel optical and radar data for mapping smallholder coffee production systems in Vietnam. *Remote Sens. Environ.* **2021**, *266*, 112709. [CrossRef]
30. Spracklen, B.; Spracklen, D.V. Synergistic Use of Sentinel-1 and Sentinel-2 to Map Natural Forest and Acacia Plantation and Stand Ages in North-Central Vietnam. *Remote Sens.* **2021**, *13*, 185. [CrossRef]
31. Phan, D.C.; Vu, B.T.; Tran, D.A.; Kha, V.T.; Nasahara, K.N. Dynamics and Determinants of Forest Changes Across Mainland Vietnam in the Recent Three Decades. *Environ. Sci. Eng.* **2023**, *1*, 527–542. [CrossRef]
32. Truong, V.T.; Hoang, T.T.; Cao, D.P.; Hayashi, M.; Tadono, T.; Nasahara, K.N. JAXA Annual Forest Cover Maps for Vietnam during 2015–2018 Using ALOS-2/PALSAR-2 and Auxiliary Data. *Remote Sens.* **2019**, *11*, 2412. [CrossRef]
33. Dung, N.T.K.; Veettil, B.K.; Bao, D.Q.; Tran, T. Environmental management in Ramsar designated wetland areas in Vietnam: Studies from U Minh Thuong and Tram Chim national parks (Mekong Delta). *Environ. Monit. Assess.* **2022**, *194*, 777. [CrossRef]
34. Pham, N.; Tran, H.; Thi, K.; Nong, A.; Rutten, M. Ecosystem Service Monitoring Using Remote Sensing, Citizen Science and Other Ground Observations and Current Practices in Vietnam. 2015. Available online: https://research.tudelft.nl/en/publications/ecosystem-service-monitoring-using-remote-sensing-citizen-science/ (accessed on 22 February 2026).
35. Tran, P.; Shaw, R. Towards an integrated approach of disaster and environment management: A case study of Thua Thien Hue province, central Viet Nam. *Environ. Hazards* **2007**, *7*, 271–282. [CrossRef]
36. Sanghvi, M.; Garde, S.; Dravid, M.; Sawant, S.; Ghosh, S. Advancements in Land Use Land Cover Classification: Deep Learning and Sentinel-2 Satellite Imagery Integration. In *Advances in Geographic Information Science*; Springer: Cham, Switzerland, 2025; Volume Part F491, pp. 245–269. [CrossRef]
37. Kumar, R.; Aneesh, K.S.; Ajay, K.V.; Murali, K.V.; Kundariati, M. Comparative Evaluation of Machine Learning Algorithms for LULC Classification Using Sentinel-1 and Sentinel-2 Imagery. In *Application of Machine Learning in Earth Sciences*; Springer: Cham, Switzerland, 2026; pp. 585–596. [CrossRef]
38. Habibie, M.I.; Nurda, N.; Fernando, D.; Arifandri, R.; Putra, P.K.; Prayogi, H.; Sencaki, D.B. Integrating Sentinel-2 and ESA world cover for effective land use and land cover assessment using machine learning. *Adv. Space Res.* **2025**, *76*, 4925–4958. [CrossRef]

39. Hagenauer, J.; Omrani, H.; Helbich, M. Assessing the performance of 38 machine learning models: The case of land consumption rates in Bavaria, Germany. *Int. J. Geogr. Inf. Sci.* **2019**, *33*, 1399–1419. [CrossRef]
40. Chaturvedi, V.; de Vries, W.T. Machine Learning Algorithms for Urban Land Use Planning: A Review. *Urban Sci.* **2021**, *5*, 68. [CrossRef]
41. Wang, J.; Bretz, M.; Dewan, M.A.A.; Delavar, M.A. Machine learning in modelling land-use and land cover-change (LULCC): Current status, challenges and prospects. *Sci. Total Environ.* **2022**, *822*, 153559. [CrossRef] [PubMed]
42. Hebryn-Baidy, L.; Rees, G. Machine Learning Algorithms Evaluated for Urban Land Use and Land Cover Classification Using Sentinel 2 Data. *Red* **2024**, *10*, 664–665.
43. Popa, A.M.; Onose, D.A.; Sandric, I.C.; Dosiadis, E.A.; Petropoulos, G.P.; Gavrilidis, A.A.; Faka, A. Using GEOBIA and Vegetation Indices to Assess Small Urban Green Areas in Two Climatic Regions. *Remote Sens.* **2022**, *14*, 4888. [CrossRef]
44. Chouhan, R.L.; Shekhawat, H.S. Land Use Land Cover Dynamics Unveiled: Machine Learning Approaches to Pixel and Object-Based Geospatial Analysis. In *International Conference on Computational Complexity and Intelligent Algorithms*; Springer: Singapore, 2026; pp. 623–634. [CrossRef]
45. Liu, B.; Du, S.; Du, S.; Zhang, X. Incorporating Deep Features into GEOBIA Paradigm for Remote Sensing Imagery Classification: A Patch-Based Approach. *Remote Sens.* **2020**, *12*, 3007. [CrossRef]
46. An, L.T.; Hung, V.V. Tourists' Intention to Revisit World Cultural Heritage Sites: An Evidence from Hue City, Vietnam. In *Olympus International Conference on Supply Chains*; Springer: Berlin/Heidelberg, Germany, 2024; pp. 119–135.
47. Hung, V.V.; Dey, S.K.; Vaculcikova, Z.; Anh, L.T.H. The influence of tourists' experience on destination loyalty: A case study of Hue City, Vietnam. *Sustainability* **2021**, *13*, 8889. [CrossRef]
48. Nguyen, T.H.H.; Cheung, C. The classification of heritage tourists: A case of Hue city, Vietnam. *J. Herit. Tour.* **2014**, *9*, 35–50.
49. Congedo, L. Semi-Automatic Classification Plugin: A Python tool for the download and processing of remote sensing images in QGIS. *J. Open Source Softw.* **2021**, *6*, 3172. [CrossRef]
50. Welcome to eCognition 10.2—eCognition | Knowledge Base. Available online: https://support.ecognition.com/hc/en-us/articles/4411809308946-Welcome-to-eCognition-10-2 (accessed on 26 April 2024).
51. Han, R.; Liu, P.; Wang, G.; Zhang, H.; Wu, X. Advantage of Combining OBIA and Classifier Ensemble Method for Very High-Resolution Satellite Imagery Classification. *J. Sens.* **2020**, *2020*, 8855509. [CrossRef]
52. El-naggar, A.M. Determination of optimum segmentation parameter values for extracting building from remote sensing images. *Alex. Eng. J.* **2018**, *57*, 3089–3097. [CrossRef]
53. Ikokou, G.B.; Smith, J.A. Technique for Optimal Selection of Segmentation Scale Parameters for Object-oriented Classification of Urban Scenes. *S. Afr. J. Geomat.* **2013**, *2*, 358–369.
54. Zhou, W. An object-based approach for urban land cover classification: Integrating LiDAR height and intensity data. *IEEE Geosci. Remote Sens. Lett.* **2013**, *10*, 928–931.
55. Gao, Y.; Mas, J.F. A Comparison of the Performance of Pixel-Based and Object-Based Classifications over Images with Various Spatial Resolutions. *Online J. Earth Sci.* **2008**, *2*, 27–35.
56. Estoque, R.C.; Murayama, Y.; Akiyama, C.M. Pixel-based and object-based classifications using high- and medium-spatial-resolution imageries in the urban and suburban landscapes. *Geocarto Int.* **2015**, *30*, 1113–1129. [CrossRef]
57. Jensen, R.R.; Hardin, P.J.; Hardin, A.J. Classification of urban tree species using hyperspectral imagery. *Geocarto Int.* **2012**, *27*, 443–458. [CrossRef]
58. Baatz, M.; Schape, A. *Multiresolution Segmentation an Optimization Approach for High Quality Multi-Scale Image Segmentation*; Strobl, J., Blaschke, T., Griesbner, G., Eds.; Angewandte Geographische Informations-Verarbeitung, XII, Wichman; Scientific Research Publishing: Irvine, CA, USA, 2000. Available online: https://www.scirp.org/reference/referencespapers?referenceid=1875442 (accessed on 29 December 2025).
59. Su, T.; Liu, T.; Zhang, S.; Qu, Z.; Li, R. Machine learning-assisted region merging for remote sensing image segmentation. *ISPRS J. Photogramm. Remote Sens.* **2020**, *168*, 89–123. [CrossRef]
60. Solano, F.; Di Fazio, S.; Modica, G. A methodology based on GEOBIA and WorldView-3 imagery to derive vegetation indices at tree crown detail in olive orchards. *Int. J. Appl. Earth Obs. Geoinf.* **2019**, *83*, 101912. [CrossRef]
61. Garcia-Pedrero, A.; Gonzalo-Martin, C.; Fonseca-Luengo, D.; Lillo-Saavedra, M. A GEOBIA Methodology for Fragmented Agricultural Landscapes. *Remote Sens.* **2015**, *7*, 767–787. [CrossRef]
62. Vlachopoulos, O.; Leblon, B.; Wang, J.; Haddadi, A.; LaRocque, A.; Patterson, G. Delineation of Crop Field Areas and Boundaries from UAS Imagery Using PBIA and GEOBIA with Random Forest Classification. *Remote Sens.* **2020**, *12*, 2640. [CrossRef]
63. Definiens, A.G. *eCognition Version 5 Object Oriented Image Analysis User Guide*; Definiens AG: Munich, Germany, 2005.
64. Choudhury, M.D.A.M.; Marcheggiani, E.; Modica, G.; Pratico, S.; Somers, B. Toward carbon neutral cities: A comparative analysis between Sentinel 2 and WorldView 3 satellite image processing for tree carbon stock mapping in Brussels. *Urban For. Urban Green.* **2024**, *101*, 128495. [CrossRef]

65. Flanders, D.; Hall-Beyer, M.; Perverzoff, J. Preliminary evaluation of eCognition object- based software for cut block delineation and feature extraction. *Can. J. Remote Sens.* **2003**, *29*, 441–452. [CrossRef]
66. Mutanga, O.; Kumar, L. Google earth engine applications. *Remote Sens.* **2019**, *11*, 591. [CrossRef]
67. Lisle, R.J. Google Earth: A new geological resource. *Geol. Today* **2006**, *22*, 29–32. [CrossRef]
68. Wong, M.M.F.; Fung, J.C.H.; Yeung, P.P.S. High-resolution calculation of the urban vegetation fraction in the Pearl River Delta from the Sentinel-2 NDVI for urban climate model parameterization. *Geosci. Lett.* **2019**, *6*, 2. [CrossRef]
69. Harrington, S.; Teitelman, J.; Rummel, E.; Morse, B.; Chen, P.; Eisentraut, D.; McDonough, D. Validating google earth pro as a scientific utility for use in accident reconstruction. *SAE Int. J. Transp. Saf.* **2017**, *5*, 135–166. [CrossRef]
70. Wang, Z.X.; Liu, C.; Tun, W.N. Google earth images based land cover data validation dataset for globeland30 (2010) in the region of roof of the world. *J. Glob. Change Data Discov.* **2019**, *3*, 259–267.
71. Dorais, A.; Cardille, J. Strategies for incorporating high-resolution google earth databases to guide and validate classifications: Understanding deforestation in Borneo. *Remote Sens.* **2011**, *3*, 1157–1176. [CrossRef]
72. Helldén, U. A Test of Landsat-2 Imagery and Digital Data for Thematic Mapping Illustrated by an Environmental Study in Northern Kenya, Lund University. 1980. Available online: https://api.semanticscholar.org/CorpusID:133990993 (accessed on 20 January 2022).
73. Immitzer, M.; Vuolo, F.; Atzberger, C. First experience with Sentinel-2 data for crop and tree species classifications in central Europe. *Remote Sens.* **2016**, *8*, 166. [CrossRef]
74. Hu, B.; Xu, Y.; Huang, X.; Cheng, Q.; Ding, Q.; Bai, L.; Li, Y. Improving Urban Land Cover Classification with Combined Use of Sentinel-2 and Sentinel-1 Imagery. *ISPRS Int. J. Geo-Inf.* **2021**, *10*, 533. [CrossRef]
75. Shi, Y.; Qi, Z.; Liu, X.; Niu, N.; Zhang, H. Urban land use and land cover classification using multisource remote sensing images and social media data. *Remote Sens.* **2019**, *11*, 2719. [CrossRef]
76. Gašparović, M.; Jogun, T. The effect of fusing Sentinel-2 bands on land-cover classification. *Int. J. Remote Sens.* **2018**, *39*, 822–841. [CrossRef]
77. Nasiri, V.; Deljouei, A.; Moradi, F.; Sadeghi, S.M.M.; Borz, S.A. Land use and land cover mapping using Sentinel-2, Landsat-8 Satellite Images, and Google Earth Engine: A comparison of two composition methods. *Remote Sens.* **2022**, *14*, 1977. [CrossRef]
78. Jagannathan, J.; Vadivel, M.T.; Divya, C. Land use classification using multi-year Sentinel-2 images with deep learning ensemble network. *Sci. Rep.* **2025**, *15*, 29047. [CrossRef]
79. Zhang, X.; Liu, L.; Zhao, T.; Zhang, W.; Guan, L.; Bai, M.; Chen, X. GLC_FCS10: A global 10 m land-cover dataset with a fine classification system from Sentinel-1 and Sentinel-2 time-series data in Google Earth Engine. *Earth Syst. Sci. Data* **2025**, *17*, 4039–4062. [CrossRef]
80. Carneiro, G.A.; Svoboda, J.; Cunha, A.; Sousa, J.J.; Štych, P. Efficient 3D convolutional neural networks for Sentinel-2 land cover classification with limited ground truth data. *Eur. J. Remote Sens.* **2025**, *58*, 2512531. [CrossRef]
81. Nolasco, M.; Balzarini, M. Assessment of temporal aggregation of Sentinel-2 images on seasonal land cover mapping and its impact on landscape metrics. *Environ. Monit. Assess.* **2025**, *197*, 142. [CrossRef]
82. Jumaah, H.J.; Rashid, A.A.; Abdul, S.; Saleh, R.; Jumaah, S.J. Deep Neural Remote Sensing and Sentinel-2 Satellite Image Processing of Kirkuk City, Iraq for Sustainable Prospective. *J. Opt. Photonics Res.* **2025**, *2*, 172–180. [CrossRef]
83. Xiong, S.; Zhang, X.; Wang, H.; Lei, Y.; Tan, G.; Du, S. Mapping the first dataset of global urban land uses with Sentinel-2 imagery and POI prompt. *Remote Sens. Environ.* **2025**, *327*, 114824. [CrossRef]
84. As-syakur, A.R.; Adnyana, I.W.S.; Arthana, I.W.; Nuarsa, I.W. Enhanced built-up and bareness index (EBBI) for mapping built-up and bare land in an urban area. *Remote Sens.* **2012**, *4*, 2957–2970. [CrossRef]
85. Ssewanyana, A.; Tu, M.C. Performance of Spectral Indices and Machine Learning Algorithms in Seasonal Classification of Urban Impervious Surfaces from Sentinel-2 Imagery: A Case Study of Taipei. *Remote Sens. Earth Syst. Sci.* **2025**, *9*, 16. [CrossRef]
86. Adrah, E.; Wong, J.P.; Yin, H. Integrating GEDI, Sentinel-2, and Sentinel-1 imagery for tree crops mapping. *Remote Sens. Environ.* **2025**, *319*, 114644. [CrossRef]
87. Godinho, S.; Corado, L.; Benevides, P.; Costa, H.; Caetano, M. Land cover mapping by combining GEDI-derived vertical metrics with SAR and multispectral data. In *Satellite Remote Sensing for Forest and Environmental Monitoring*; Elsevier: Amsterdam, The Netherlands, 2026; pp. 185–220. [CrossRef]
88. Luong, N.D.; Khuc, T.D.; Vu, D.C. Comparison of boosting algorithms for land cover mapping using object-based classification. *Rev. Teledetección.* **2026**, *67*. [CrossRef]
89. Abdelkareem, M.; Mansour, A.M. Land Use/Land Cover Spatiotemporal Change Detection Using Landsat, Sentinel and SPOT Imageries. *Remote Sens. Earth Syst. Sci.* **2025**, *9*, 12. [CrossRef]
90. Zhang, P.; Ke, Y.; Zhang, Z.; Wang, M.; Li, P.; Zhang, S. Urban land use and land cover classification using novel deep learning models based on high spatial resolution satellite imagery. *Sensors* **2018**, *18*, 3717. [CrossRef]
91. Kuras, A.; Brell, M.; Rizzi, J.; Burud, I. Hyperspectral and lidar data applied to the urban land cover machine learning and neural-network-based classification: A review. *Remote Sens.* **2021**, *13*, 3393. [CrossRef]

92. Man, Q.; Dong, P.; Guo, H. Pixel-and feature-level fusion of hyperspectral and lidar data for urban land-use classification. *Int. J. Remote Sens.* **2015**, *36*, 1618–1644. [CrossRef]
93. Cao, Q.; Zhong, Y.; Ma, A.; Zhang, L. Urban land use/land cover classification based on feature fusion fusing hyperspectral image and LiDAR data. In *IGARSS 2018-2018 IEEE International Geoscience and Remote Sensing Symposium*; IEEE: Valencia, Spain, 2018; pp. 8869–8872.
94. da Silveira, H.L.F.; Galvão, L.S.; Sanches, I.D.; de Sá, I.B.; Taura, T.A. Use of MSI/Sentinel-2 and airborne LiDAR data for mapping vegetation and studying the relationships with soil attributes in the Brazilian semi-arid region. *Int. J. Appl. Earth Obs. Geoinf.* **2018**, *73*, 179–190. [CrossRef]
95. Hummel, S.; Hudak, A.T.; Uebler, E.H.; Falkowski, M.J.; Megown, K.A. A comparison of accuracy and cost of LiDAR versus stand exam data for landscape management on the Malheur National Forest. *J. For.* **2011**, *109*, 267–273. [CrossRef]
96. Buying Satellite Imagery: Pricing Information for High Resolution Satellite Imagery. Available online: https://landinfo.com/satellite-imagery-pricing/ (accessed on 15 April 2025).
97. Hansch, R.; Hellwich, O. Fusion of Multispectral LiDAR, Hyperspectral, and RGB Data for Urban Land Cover Classification. *IEEE Geosci. Remote Sens. Lett.* **2021**, *18*, 366–370. [CrossRef]
98. Godwin, C.; Chen, G.; Singh, K.K. The impact of urban residential development patterns on forest carbon density: An integration of LiDAR, aerial photography and field mensuration. *Landsc. Urban Plan.* **2015**, *136*, 97–109. [CrossRef]
99. Rasti, B.; Ghamisi, P.; Gloaguen, R. Fusion of Multispectral LiDAR and Hyperspectral Imagery. In *International Geoscience and Remote Sensing Symposium (IGARSS)*; Institute of Electrical and Electronics Engineers Inc.: Piscataway, NJ, USA, 2020; pp. 2659–2662. [CrossRef]
100. Topaloğlu, R.H.; Aksu, G.A.; Ghale, Y.A.G.; Sertel, E. High-resolution land use and land cover change analysis using GEOBIA and landscape metrics: A case of Istanbul, Turkey. *Geocarto Int.* **2022**, *37*, 9071–9097. [CrossRef]
101. Ma, L.; Li, M.; Ma, X.; Cheng, L.; Du, P.; Liu, Y. A review of supervised object-based land-cover image classification. *ISPRS J. Photogramm. Remote Sens.* **2017**, *130*, 277–293. [CrossRef]
102. Gun, Z.; Chen, J. Novel Knowledge Graph- and Knowledge Reasoning-Based Classification Prototype for OBIA Using High Resolution Remote Sensing Imagery. *Remote Sens.* **2023**, *15*, 321. [CrossRef]
103. Chen, G.; Weng, Q.; Hay, G.J.; He, Y. Geographic object-based image analysis (GEOBIA): Emerging trends and future opportunities. *GIsci. Remote Sens.* **2018**, *55*, 159–182. [CrossRef]
104. Zhang, X.; Du, S.; Wang, Q. Integrating bottom-up classification and top-down feedback for improving urban land-cover and functional-zone mapping. *Remote Sens. Environ.* **2018**, *212*, 231–248. [CrossRef]
105. Du, S.; Shu, M.; Wang, Q. Modelling relational contexts in GEOBIA framework for improving urban land-cover mapping. *GIsci. Remote Sens.* **2019**, *56*, 184–209. [CrossRef]